ICASE

A NUMERICAL METHOD FOR COMPUTING THE SHAPE OF

A VERTICAL SLENDER JET

John Strikwerda

James Geer

Report No. 80-7

March 24, 1980

INSTITUTE FOR COMPUTER APPLICATIONS IN SCIENCE AND ENGINEERING

NASA Langley Research Center, Hampton, Virginia

Operated by the

UNIVERSITIES SPACE USRA RESEARCH ASSOCIATION

A NUMERICAL METHOD FOR COMPUTING THE SHAPE OF A VERTICAL SLENDER JET

John Strikwerda
Institute for Computer Applications in Science and Engineering
James Geer
State University of New York at Binghamton

ABSTRACT

A numerical method is presented for computing the shape of a vertical slender jet of fluid falling steadily under the force of gravity. The problem being solved is formulated as a nonlinear free boundary value problem for the cross-sectional shape of the jet. The numerical method of solution treats the boundary conditions of the problem as a pair of nonlinear hyperbolic pseudo-differential equations to be integrated in the stream-wise direction. The original differential equation appears as an auxiliary condition. This formulation is shown to be well-posed. The numerical method is found to be stable and second order accurate. Computations are presented for jets issuing from several different orifice shapes. The numerical method of solution appears to be new and may be applicable to other nonlinear free boundary value problems.

The first author was supported under NASA Contract No. NAS1-15810 while he was in residence at ICASE, NASA Langley Research Center, Hampton, VA 23665. The research for the second author was partially supported by the Research Foundation of S.U.N.Y. under Contract No. 240-6135A and partially supported under NASA Contract No. NAS1-15810.

1. Introduction

We present in this paper a numerical method which we have used to determine the shape of the free surface of a slender jet of fluid falling vertically in the presence of gravity. The flow is assumed to be a steady, three-dimensional potential flow. The solution procedure determines the cross-sectional shape given the shape and velocity profile at a particular height (e.g., at an orifice from which the jet emanates). Surface tension and viscous effects are neglected. The mathematical formulation of the problem leads to a fully three-dimensional, nonlinear boundary value problem for Laplace's equation, for which the boundary of the flow is also unknown. For the case of a slender jet, however, Tuck (1976) and Geer (1977a,b) derived equations to describe the first approximations to the cross-sectional shape and velocities of the jet. The problem of determining the shape is thus reduced to solving a nonlinear two-dimensional problem in the cross-sectional plane of the jet. Both Tuck and Geer gave an exact solution to this problem for a jet with an elliptical cross-sectional shape. (See also Green (1977).) To date no other exact solutions have been found.

The purpose of this work is to present in some detail the method we have developed to solve numerically the associated nonlinear free boundary value problem for jets which fall vertically from an orifice of a specified shape. The problem is formulated in section 2 and then transformed into a form more suitable for numerical integration. In sections 3-5, we describe the numerical method that we have used to integrate the problem outlined in section 2.

In section 6 we present the results for three of the different orifice shapes for which our calculations were made. These shapes are an ellipse, a rectangle, and an equilateral triangle. The accuracy of our method is discussed in section 7, while the well-posedness and stability of the method are discussed in section 8.

The numerical method presented here appears to be new and may be applicable to other three-dimensional free boundary value problems. The usefulness of most existing numerical methods for solving free boundary value problems is restricted to one and two dimensions (see Wilson, et al (1978)).

2. Formulation of the Problem

Let the velocity potential of the jet be denoted by $\Phi = \Phi(r,\theta,z;\varepsilon)$ and let the shape of the free surface of the jet be described by $r = S(\theta,z;\varepsilon)$ (see Figure 1). Here r, θ, and z form the usual (non-dimensional) cylindrical coordinate system, with the positive z-axis pointing vertically downward in the direction of gravity. The parameter ε, the slenderness ratio of the jet, is the ratio of a typical radius of the jet to a typical length along the jet and is defined precisely by Geer (1977a). The boundary conditions at the free surface are the kinematic condition of no flow through the surface and Bernoulli's equation with constant pressure. For small values of ε, Geer (1977a) has shown that Φ and S are given by

$$\Phi = \tfrac{2}{3}(1+z)^{\frac{3}{2}} + \varepsilon^2\phi(r,\theta,z) + O(\varepsilon^3) \quad , \tag{2.1}$$

$$S = S(\theta,z) + O(\varepsilon) \quad , \tag{2.2}$$

where ϕ and S satisfy the conditions

$$\frac{\partial^2\phi}{\partial r^2} + \frac{1}{r}\frac{\partial\phi}{\partial r} + \frac{1}{r^2}\frac{\partial^2\phi}{\partial\theta^2} = -\tfrac{1}{2}(1+z)^{-\frac{1}{2}} \quad , \quad z>0, \quad 0\leq r<S(\theta,z) \quad , \tag{2.3}$$

with

$$\frac{\partial\phi}{\partial r} - \frac{1}{S^2}\frac{\partial S}{\partial\theta}\frac{\partial\phi}{\partial\theta} = (1+z)^{\frac{1}{2}}\frac{\partial S}{\partial z} \tag{2.4}$$

and

$$\left(\frac{\partial\phi}{\partial r}\right)^2 + S^{-2}\left(\frac{\partial\phi}{\partial\theta}\right)^2 + 2(1+z)^{\frac{1}{2}}\frac{\partial\phi}{\partial z} = 0 \tag{2.5}$$

holding on $r = S(\theta,z)$. Equation (2.3) follows from Laplace's equation for the potential while equations (2.4) and (2.5) result from the substitution of the perturbation expansions (2.1) and (2.2) in the boundary conditions. Thus, we see that ϕ must satisfy the two-dimensional Poisson equation (2.3) in the cross-section of the jet, while equation (2.4) essentially prescribes the normal derivative of ϕ at the boundary of the cross-section. Equation (2.5) is the additional condition which is needed to determine the free surface. In particular, it is an easy exercise to show that an initially circular jet with a uniform velocity profile has cross-sections which remain circular and decrease in area as the jet accelerates.

To compute ϕ and S, we transform the problem (2.3)-(2.5) into a form that is somewhat easier to deal with numerically. We first note that we can easily find a particular solution to (2.3) and consequently we write ϕ in the form

$$\phi = -\tfrac{1}{8}(1+z)^{-\frac{1}{2}}r^2 + \psi \quad , \tag{2.6}$$

where ψ satisfies the homogeneous version of equation (2.3), i.e., Laplace's equation. Both ψ and S are presumed known at $z = 0$. We then introduce a new independent radial variable ρ, related to r by

$$\rho = \frac{r}{S(\theta,z)} \quad . \tag{2.7}$$

Thus, r is stretched in a non-uniform manner, but the unknown boundary $r = S(\theta,z)$ is mapped onto the known boundary $\rho = 1$. We also define the new dependent variable $R(\theta,z)$ by

$$R(\theta,z) = \tfrac{1}{2}\, S(\theta,z)^2 (1+z)^{\frac{1}{2}} \quad . \tag{2.8}$$

In terms of the independent variables ρ, θ, and z, and the dependent variables $\psi(\rho,\theta,z)$ and $R(\theta,z)$, equations (2.4) and (2.5) can be written as

$$\frac{\partial R}{\partial z} = (1+\beta^2)\, \frac{\partial \psi}{\partial \rho} - \beta \frac{\partial \psi}{\partial \theta} \tag{2.9}$$

$$4R\, \frac{\partial \psi}{\partial z} = (1+\beta^2) \left(\frac{\partial \psi}{\partial \rho}\right)^2 - \left(\frac{\partial \psi}{\partial \theta}\right)^2 - \frac{3}{4}\, \frac{R^2}{(1+z)^2} \quad , \tag{2.10}$$

where $\beta = \frac{1}{S}\frac{\partial S}{\partial \theta} = \frac{1}{2}\frac{1}{R}\frac{\partial R}{\partial \theta}$. These equations hold for $\rho = 1$, $0 \le \theta \le 2\pi$, and $z > 0$. The differential equation (2.3) then becomes

$$(1+\beta^2)\, \frac{1}{\rho}\frac{\partial}{\partial \rho}\left(\rho \frac{\partial \psi}{\partial \rho}\right) - \frac{\partial \beta}{\partial \theta}\frac{1}{\rho}\frac{\partial \psi}{\partial \rho} + \frac{1}{\rho^2}\frac{\partial^2 \psi}{\partial \theta^2} - 2\beta\, \frac{1}{\rho}\frac{\partial^2 \psi}{\partial \rho \partial \theta} = 0 \tag{2.11}$$

$$0 \le \theta \le 2\pi \quad , \qquad 0 \le \rho < 1 \quad , \qquad z \ge 0 \quad .$$

As a consequence of equations (2.3) - (2.5), we find the integrability condition

$$\int_0^{2\pi} R(\theta,z)d\theta = \text{constant} = 2\pi\bar{M} \tag{2.12}$$

which expresses the constant mass flux in the jet.

Thus, we seek solutions to equations (2.9) - (2.11) for ψ and R in the region $0 \leq \rho \leq 1$, $z > 0$. Once ψ and R have been found, ϕ and S can be recovered using (2.6) and (2.8).

3. Method of Solution

In this and the next two sections, we shall describe the method we have devised to solve the problem formulated in section 2. In particular, in this section we will present the underlying motivation for our method as well as the specific finite difference formulas we use. Details of the method we use to solve Laplace's equation will be discussed in the next section, while our treatment of possible discontinuities (e.g. corners) in the jet profile shape will be presented in section 5.

Instead of attempting to solve the differential equation (2.11) subject to the auxiliary conditions (2.9) - (2.10) and (2.12) (as in a classical approach), we proceed in a different manner. To begin, we temporarily think of both ψ and R as functions of z and θ, defined only on the boundary $\rho = 1$. Then, in this context, we may regard equations (2.9) - (2.10) as a system of two nonlinear hyperbolic pseudo-differential equations for ψ and R, with z being the time-like variable and θ the spatial variable. These equations are hyperbolic because the first-order symbol of the linearized system has purely imaginary eigenvalues (see section 8). They are "pseudo" differential equations because the operator $\frac{\partial}{\partial\rho}$ is a non-local operator on ψ, when considered as defined only on $\rho = 1$. However, the "auxiliary" condition (2.11) which holds for $\rho < 1$ serves to define $\frac{\partial\psi}{\partial\rho}$ in terms of ψ and R on the boundary. Condition (2.12) is then a conservation law

In order to obtain a numerical approximation to the solution of our problem formulated in this manner, we use a finite difference scheme defined on the grid points as follows:

$$\begin{aligned} \theta_i &= (i-1)\,\Delta\theta \qquad && i=1,\ldots,N \ , \\ \rho_j &= 1-(j-1)\,\Delta\rho \qquad && j=1,\ldots,M \ , \\ z_n &= n\,\Delta z \qquad && n=0,\ 1,\ 2,\ 3,\ldots \ , \end{aligned} \tag{3.1}$$

where $\Delta\theta = 2\pi/(N-1)$, $\Delta\rho = 1/(M-1)$, and Δz is chosen to satisfy appropriate stability and accuracy criteria (see sections 7 and 8). Note that $\theta_1 = 0$, $\theta_N = 2\pi$, $z_0 = 0$, $\rho_1 = 1$ and $\rho_M = 0$. We then use the MacCormack scheme (MacCormack (1969)) to solve equations (2.9) - (2.10). In particular, if we define the vector $\vec{w}(\theta,z)$ by $\vec{w} = (R,\psi)^T$, then equations (2.9) - (2.10) can be written as

$$\frac{\partial \vec{w}}{\partial z} = \vec{F}\left(z, \vec{w}, \frac{\partial \vec{w}}{\partial \theta}, \frac{\partial \psi}{\partial \rho}\right) \ , \tag{3.2}$$

where the form of the vector $\vec{F}$ can be determined from the right-hand sides of (2.9) - (2.10). We employ the forward and backward difference operators, D_+ and D_-, respectively, defined by

$$\begin{aligned} D_+\vec{w}_i^n &= (\vec{w}_{i+1}^n - \vec{w}_i^n)/\Delta\theta \ , \\ D_-\vec{w}_i^n &= (\vec{w}_i^n - \vec{w}_{i-1}^n)/\Delta\theta \ , \\ \vec{w}_i^n &= \vec{w}(\theta_i, z_n) \ . \end{aligned} \tag{3.3}$$

Then the forward-backward MacCormack scheme we use is given by the following two-step formula:

$$\text{(predictor):} \qquad \tilde{\vec{w}}_i^{n+1} = \vec{w}_i^n + \Delta z \vec{F}\left(z_n, \vec{w}_i^n, D_+\vec{w}_i^n, D_\rho \psi_i^n\right) \tag{3.4}$$

$$\text{(corrector):} \qquad \vec{w}_i^{n+1} = \tfrac{1}{2}\left\{\vec{w}_i^n + \tilde{\vec{w}}_i^{n+1} + \Delta z \vec{F}(z_{n+1}, \tilde{\vec{w}}_i^{n+1}, D_-\tilde{\vec{w}}_i^{n+1}, D_\rho \tilde{\psi}_i^{n+1})\right\}. \tag{3.5}$$

Here $D_\rho \psi_i^n$ is an approximation to $\frac{\partial \psi}{\partial \rho}$ on $\rho = 1$ at $\theta = \theta_i$ and $z = z_n$, which we shall describe below. In order to maintain symmetry, the forward-backward MacCormack scheme is alternated with the backward-forward scheme, which uses backward differences in the predictor step and forward differences in the corrector step. Also, it was found that the conservation law (2.12) was satisifed more closely when the quantity β in equations (2.9) and (2.10) was approximated as

$$D_\pm R_i^n / (R_i^n + R_{i\pm1}^n)$$

and this form was used in all the calculations given here.

The term $D_\rho \psi_i^n$ in (3.4) and (3.5) is computed by first solving for an approximation to the solution ψ of (2.11), with ψ_i^n specified on the boundary. The approximation is given by

$$\begin{aligned} &A_i^n \rho_j \left[\rho_{j-\frac{1}{2}}(\psi_{i,j-1} - \psi_{i,j}) - \rho_{j+\frac{1}{2}}(\psi_{i,j} - \psi_{i,j+1})\right](\Delta\rho)^{-2} \\ &- C_i^n \rho_j (\psi_{i,j-1} - \psi_{i,j+1})(2\Delta\rho)^{-1} + (\psi_{i+1,j} - 2\psi_{i,j} + \psi_{i-1,j})(\Delta\theta)^{-2} \\ &- \rho_j \Big\{ B_{i+}^n [\psi_{i+1,j-1} - \psi_{i,j-1} - \psi_{i+1,j+1} + \psi_{i,j+1}] \\ &+ B_{i-}^n (\psi_{i,j-1} - \psi_{i-1,j-1} - \psi_{i,j+1} + \psi_{i-1,j+1}) \Big\} (2\Delta\rho\Delta\theta)^{-1} = 0 . \end{aligned} \tag{3.6}$$

Here, $\psi_{i,j} = \psi^n_{i,j} = \psi(\rho_j, \theta_i, z_n)$, and

$$
\begin{aligned}
B^n_{i\pm} &= (D_{\pm} R^n_i)/(R^n_i + R^n_{i\pm 1}) \quad , \\
A^n_i &= 1 + \tfrac{1}{2}\left[(B^n_{i+})^2 + (B^n_{i-})^2 \right] \quad , \\
C^n_i &= (B^n_{i+} - B^n_{i-})/\Delta\theta \quad .
\end{aligned}
\tag{3.7}
$$

In equations (3.6) and (3.7) we have used second order accurate difference approximations to the derivatives of ψ and R. Equations (3.6) are solved by successive over-relaxation (see section 4). Once $\psi^n_{i,j}$ is determined the term $D_\rho \psi^n_i$ is computed as

$$
D_\rho \psi^n_i = (3\psi^n_{i,1} - 4\psi^n_{i,2} + \psi^n_{i,3})/2\Delta\rho \quad , \tag{3.8}
$$

which is a second-order one-sided approximation to $\frac{\partial \psi}{\partial \rho}$.

Equations (3.1) - (3.8) describe our numerical scheme to solve the problem of section 2. For each z step, equations (3.6) are solved twice, once corresponding to the predictor steps (3.4) and then again for the corrector step (3.5). The fact that our scheme is formally second order accurate will be shown below. In section 7, the second order accuracy of our method is confirmed by the results of several numerical experiments.

We conclude this section by showing that the scheme given by equations (3.4) - (3.5) is formally second-order accurate. To do this, we note that if $\vec{w}$ is a smooth function of z then by Taylor's theorem

$$\vec{w}(z_{n+1}) = \vec{w}(z_n) + \Delta z \frac{\partial \vec{w}}{\partial z}(z_n) + \frac{(\Delta z)^2}{2} \frac{\partial^2 \vec{w}}{\partial z^2} + 0((\Delta z)^3) \quad . \tag{3.9}$$

Let $\Delta\theta$ and $\Delta\rho$ be proportional to Δz and for convenience set

$$\vec{w}^n = \vec{w}(1,\theta,z_n) \ ,$$

$$\vec{p}_{\pm}^{\,n} = D_{\pm}\vec{w}^n \ ,$$

$$q^n = D_\rho \psi(1,\theta,z_n) \ ,$$

$$\vec{F}_{\pm}^{\,n} = \vec{F}(z_n, \vec{w}^n, \vec{p}_{\pm}^{\,n}, q^n) \ .$$

Then, from (3.2)

$$\frac{\partial \vec{w}}{\partial z}(z_n) = \vec{F}(z_n, \vec{w}^n, \frac{\partial \vec{w}^n}{\partial \theta}, D_\rho \psi^n) = \tfrac{1}{2}\left\{\vec{F}_+^n + \vec{F}_-^n\right\} + 0((\Delta z)^2) \quad , \tag{3.10}$$

and

$$\begin{aligned} \Delta z \frac{\partial^2 \vec{w}}{\partial z^2}(z_n) &= \Delta z \frac{\partial}{\partial z}\left\{\vec{F}(z_n, \vec{w}^n, \vec{p}_-^{\,n}, q^n) + 0(\Delta z)\right\} \\ &= \Delta z \frac{\partial \vec{F}_-}{\partial z} + \frac{\partial \vec{F}_-}{\partial \vec{w}} \Delta \vec{w}^n \\ &\quad + \frac{\partial \vec{F}_-}{\partial \vec{p}_-} \Delta \vec{p}^{\,n} + \frac{\partial \vec{F}_-}{\partial q} \Delta q^n + 0((\Delta z)^2) \quad , \end{aligned} \tag{3.11}$$

where $\Delta \vec{w}^n = \vec{w}^{n+1} - \vec{w}^n$, etc.

If $\tilde{\vec{w}}^{n+1}$ is defined by the right side of (3.4), i.e. the predicted value of $\vec{w}^{n+1}$, and

$$\tilde{\vec{p}}_-^{n+1} = D_- \tilde{\vec{w}}^{n+1} \quad , \quad \text{and} \quad \tilde{q}^{n+1} = D_\rho \tilde{\psi}(1,\theta,z_{n+1}) \quad ,$$

then

$$\Delta \vec{w}^n = \tilde{\vec{w}}^{n+1} - \vec{w}^n + 0((\Delta z)^2) \quad ,$$

$$\Delta \vec{p}_-^{\,n} = \tilde{\vec{p}}_-^{n+1} - \vec{p}_-^{\,n} + 0((\Delta z)^2) \quad ,$$

$$\Delta q^n = \tilde{q}^{n+1} - q^n + 0((\Delta z)^2) \quad . \tag{3.12}$$

Substituting equations (3.10) - (3.12) into (3.9), we obtain

$$\vec{w}(z_{n+1}) = \vec{w}(z_n) + \frac{\Delta z}{2} \vec{F}_+^n + \frac{\Delta z}{2} \left\{ \vec{F}_-^n + \Delta z \left[\frac{\partial \vec{F}^n}{\partial z} + \frac{\partial \vec{F}}{\partial \vec{w}} (\tilde{\vec{w}}^{n+1} - \vec{w}^n) \right.\right.$$

$$\left.\left. + \frac{\partial \vec{F}}{\partial \vec{p}} (\tilde{\vec{p}}^{n+1} - \vec{p}^n) + \frac{\partial \vec{F}}{\partial q} (\tilde{q}^{n+1} - q^n) \right] \right\} + 0((\Delta z)^3)$$

$$= \tfrac{1}{2} \left\{ \vec{w}(z_n) + [\vec{w}(z_n) + \Delta z \, \vec{F}_+^n] \right.$$

$$\left. + \Delta z \, \vec{F}(z_{n+1}, \tilde{\vec{w}}^{n+1}, \tilde{\vec{p}}_-^{n+1}, \tilde{q}^{n+1}) \right\} + 0((\Delta z)^3) \quad ,$$

which is equivalent to equations (3.4) - (3.5), and shows that the scheme is formally second order accurate.

4. Solution of Laplace's Equation

To use the difference scheme (3.1) - (3.8) to advance the solution from $z = z_n$ to $z = z_{n+1}$ requires solving the difference approximation (3.6) to Laplace's equation for both the predictor and corrector steps. The values of ψ^n and $\tilde{\psi}^{n+1}$ in the interior (i.e., $\rho < 1$) are used with formula (3.8)

to compute $D_\rho \psi^n$ and $D_\rho \tilde{\psi}^{n+1}$, respectively, which are the approximations to the normal derivative of ψ at $\rho = 1$.

The difference approximation (3.6) to Laplace's equation is solved by point successive over-relaxation (SOR) using the natural ordering of grid points. The SOR algorithm is given by

$$\begin{aligned}\psi_{i,j}^{,k+1} = \psi_{i,j}^{,k} + \tilde{\omega}_i \Big\{ & A_i \rho_j \left(\rho_{j-\frac{1}{2}} \left(\psi_{i,j-1}^{,k+1} - \psi_{i,j}^{,k} \right) - \rho_{j+\frac{1}{2}} \left(\psi_{i,j}^{,k} - \psi_{i,j+1}^{,k} \right) \right) \Delta\rho \\ & - C_i \rho_j \left(\psi_{i,j-1}^{,k+1} - \psi_{i,j+1}^{,k} \right) (2\Delta\rho)^{-1} \\ & + \left(\psi_{i+1,j}^{,k} - 2\psi_{i,j}^{,k} + \psi_{i,j+1}^{,k+1} \right) (\Delta\theta)^{-2} \\ & - \rho_j \Big\{ B_{i+} \left[\psi_{i+1,j-1}^{,k+1} - \psi_{i,j-1}^{,k+1} - \psi_{i+1,j+1}^{,k} + \psi_{i,j+1}^{,k} \right] \\ & + B_{i-} \left[\psi_{i,j-1}^{,k+1} - \psi_{i-1,j-1}^{,k+1} - \psi_{i,j+1}^{,k} + \psi_{i-1,j+1}^{,k} \right] \Big\} (2\Delta\rho\Delta\theta)^{-1} \Big\} \end{aligned} \tag{4.1}$$

$$j = 1, \ldots, N-1,$$

$$j = 2, \ldots, M-1,$$

where, to simplify notation, we write $\psi_{i,j}^{,k}$ for the k^{th} iterate for either $\psi_{i,j}^{n}$ or $\tilde{\psi}_{i,j}^{n+1}$. The iteration parameter $\tilde{\omega}_i$ is given by

$$\tilde{\omega}_i = \tfrac{1}{2}\, \omega \Big/ \left(A_i \left(\frac{\rho}{\Delta\rho} \right)^2 + \left(\frac{1}{\Delta\theta} \right)^2 \right) \tag{4.2}$$

where

$$\omega = 2 / \left(1 + 2.4 \bar{M}^{-1/2} (1+z)^{1/4} \Delta\rho \right), \tag{4.3}$$

and $\bar{M}$ is defined by equation (2.12). Formula (4.2) is a normalization, dividing the standard SOR parameter ω by the absolute value of the coefficient of $\psi_{i,j}$ in the approximation (3.6).

Formula (4.3) giving the SOR parameter ω will be discussed later in this section. The coefficients A_i, $B_{i\pm}$, and C_i are functions of R_i^n or $\tilde{R}_i^{n+1}$ and are given by formulas (3.7).

The value of $\psi^{,k+1}$ at the origin, i.e. $\psi_{i,M}^{,k+1}$, was determined from the values at the neighboring grid points, $\psi_{i,M-1}^{,k+1}$, by means of the formula

$$\psi_{i,M}^{,k+1} = \sum_{i=1}^{N-1} (A_i + C_i)\, \psi_{i,M-1}^{,k+1} \Big/ \sum_{i=1}^{N-1} (A_i + C_i) \ . \qquad (4.4)$$

Formula (4.4) is derived by integrating Laplace's equation (2.11) over a disc of radius ε centered at the origin. This gives

$$\varepsilon \int_0^{2\pi} (1+\beta^2)\, \frac{\partial \psi}{\partial \rho}\, (\varepsilon,\theta)\, d\theta + \int_0^{2\pi} \frac{\partial \beta}{\partial \theta}\, \psi(\varepsilon,\theta)\, d\theta = 0 \ . \qquad (4.5)$$

If ε is taken to be $\frac{1}{2}\Delta\rho$ and the integrals are approximated by sums while the integrands are approximated as

$$\frac{\partial \psi}{\partial \rho}\, (\tfrac{1}{2}\Delta\rho_j, \theta_i) \simeq (\psi_{i,M-1} - \psi_{i,M})/\Delta\rho \ ,$$

and

$$\psi(\tfrac{1}{2}\Delta\rho_j, \theta_i) \simeq (\psi_{i,M-1} + \psi_{i,M})/2 \ ,$$

then equation (4.5) yields

$$\sum_{i=1}^{N-1} A_i\, (\psi_{i,M-1} - \psi_{i,M}) + \sum_{i=1}^{N-1} C_i\, (\psi_{i,M-1} + \psi_{i,M}) = 0 \ . \qquad (4.6)$$

Here, as in equations (3.7),

$$A_i \simeq 1+\beta_i^2 \quad , \qquad C_i \simeq \frac{\partial}{\partial\theta}\beta\,(\theta_i) \quad .$$

Since $\psi_{i,M}$ is independent of θ_i and

$$\sum_{i=1}^{N-1} C_i = \sum_{i=1}^{N-1} \left(\frac{R_{i+1} - R_i}{R_{i+1} + R_i} - \frac{R_i - R_{i-1}}{R_i + R_{i-1}} \right) \Delta\theta^{-2} = 0 \ ,$$

formula (4.4) follows easily from formula (4.6). Note that formula (4.4) is formally second-order accurate, as is the approximation (3.6).

After equations (4.1) and (4.4) where applied for $i < N$, the periodicity conditions

$$\psi_{N,j}^{,k+1} = \psi_{1,j}^{,k+1} \ , \quad 1 \le j \le M \ , \tag{4.7}$$

were imposed. The iterative procedure given by formulas (4.1) - (4.4) was terminated when certain convergence criteria were satisfied. These criteria will be discussed later in this section.

As noted at the beginning of this section, the approximation to Laplace's equation must be solved twice to advance the solution by one z-step. Solving these difference equations is the most time consuming portion of the algorithm. By using linear extrapolation to obtain the initial iterate for the predictor step the solution time was reduced dramatically. In particular, for the predictor step, the values of $\tilde{\psi}_{i,j}^{n+1,0}$, the starting values for the iteration, were obtained as

$$\tilde{\psi}_{i,j}^{n+1,0} = 2\psi_{i,j}^{n} - \psi_{i,j}^{n-1} \qquad \begin{matrix} i = 1,\ldots,N \\ j = 2,\ldots,M \end{matrix} \tag{4.8}$$

for the interior values. The values of $\tilde{\psi}^{n+1}_{i,1}$ on the boundary were given by equation (3.4). For the corrector step the initial iterates were taken to be the values of the predicted potential in the interior, i.e.

$$\psi^{n+1,0}_{i,j} = \tilde{\psi}^{n+1}_{i,j} \quad , \quad i = 1,\ldots,N \qquad (4.9)$$
$$j = 2,\ldots,M \ .$$

The values of $\psi^{n+1}_{i,1}$ on the boundary are, of course, given by formula (3.5).

For both the predictor and corrector steps the SOR procedure was terminated when the relative change between iterates measured in the ℓ^2-norm was less then a small parameter, ε, i.e. when

$$||\tilde{\psi}^{n+1,k} - \tilde{\psi}^{n+1,k-1}|| \leq \varepsilon \, ||\tilde{\psi}^{n+1,k}||. \qquad (4.10)$$

Then we set

$$\tilde{\psi}^{n+1}_{i,j} = \tilde{\psi}^{n+1,k}_{i,j}$$

and similarly for ψ^{n+1}. For the computations described in this paper ε was taken to be 10^{-5}. The number of iterations to compute either $\tilde{\psi}^{n+1}$ or ψ^{n+1} was restricted to be less than 250. When this limit was achieved, the last iterate was taken to be the solution. This limit was encountered only for $z = \Delta z$ (and sometimes for $2\Delta z$) when $||\tilde{\psi}||_2$ and $||\psi||_2$ were very small, or for larger values of z when the solution was no longer well behaved due to lack of resolution (see section 6). Since for our examples the potential ψ is zero at $z = 0$, the condition (4.10) is not very appropriate for small values of n.

Typical values for the number of SOR iterations required to solve for the potential are given in Table I. Column a) gives the number of

iterations when the linear extrapolation (4.8) was used for the predictor step and column b) gives the number of iterations when the initial values for the predictor step were the values of potential at the previous values of z, i.e,

$$\tilde{\psi}_{i,j}^{n+1,0} = \psi_{i,j}^{n} \quad . \tag{4.11}$$

Note that the total number of iterations per step using (4.11) is more than five times that required when the linear extrapolation (4.8) is used. This reduction in time more than justifies the extra storage required to keep the values of ψ^{n-1}.

The formula (4.3) for the iteration parameter ω was obtained in the following way. The difference equations (3.6) are a second-order approximation to Laplace's equation on the region $r \leq S(\theta,z)$ with a non-uniform grid given by equations (3.1). For the usual second-order accurate five-point difference approximation for Laplace's equation on a regular mesh, Garabedian (1956) showed that the optimal iteration parameter for SOR is given approximately by

$$\omega = \frac{2}{1+k_1 h/\sqrt{2}} \quad , \tag{4.12}$$

where h is the mesh width and k_1 is the first eigenvalue of the Laplacian on the domain being considered. He also pointed out that the value of k_1 can be estimated from below by the Faber-Krahn inequality

$$k_1 \geq 2.4 \left(\frac{\pi}{A}\right)^{1/2} = \tilde{k}_1$$

where A is the area of the domain.

In the present case, the cross-sectional area A varies as a function of z and is given by

$$A = 2\pi\bar{M}(1+z)^{-1/2}$$

where $\bar{M}$ is defined by equation (2.12). Thus we have

$$\tilde{k}_1 = (1.2)\sqrt{2}\,\bar{M}^{-1/2}\,(1+z)^{1/4} \quad .$$

Using this as an estimate for k_1 in equation (4.11), we find

$$\omega = \frac{2}{1+1.2\,\bar{M}^{-1/2}\,(1+z)^{1/4}\,h} \quad .$$

In the present context it is not clear what value should be given to h. On intuitive grounds it was taken to be proportional to $\Delta\rho$. Moreover, the Faber-Krahn inequality is sharp for circular domains and is less accurate for elongated and non-convex domains. Thus, the quantity $k_1 h$ in formula (4.12) was estimated by multiples of $\tilde{k}_1\Delta\rho$ and, after some experimentation, it was found that $2\tilde{k}_1\Delta\rho$ or $\tilde{k}_1\Delta\rho$ worked very well in most of the computations considered in this paper.

5. The Treatment of Corners

The scheme (3.1) - (3.8) was used to compute the shape of jets whose cross-sectional shapes contained corners or cusps. Examples of such jets are those which emanate from rectangular or triangular orifices. In this section we will examine the finite difference approximation to the solution in the vicinity of such corners.

For this purpose, consider a corner such as that illustrated in Figure 2 and assume that R and ψ are symmetric about the corner,

that is,

$$R(\theta_0 + \theta) = R(\theta_0 - \theta)$$

$$\psi(\theta_0 + \theta) = \psi(\theta_0 - \theta)$$

where θ_0 is the angular coordinate of the corner. At such a corner $\partial R/\partial\theta$ and $\frac{\partial\psi}{\partial\theta}$ will change sign, i.e.

$$\frac{\partial R}{\partial\theta} \quad (\theta_0 + \theta) = - \frac{\partial R}{\partial\theta} \quad (\theta_0 - \theta)$$

$$\frac{\partial\psi}{\partial\theta} \quad (\theta_0 + \theta) = - \frac{\partial\psi}{\partial\theta} \quad (\theta_0 - \theta)$$

and $\partial R/\partial\theta$ will be discontinuous. (Recall that R is related to the shape function S by equation (2.8).) However, notice that these discontinuous quantities appear in equations (2.9) - (2.10) only as products or squares (recall that $\beta = \frac{1}{2R}\frac{\partial R}{\partial\theta}$) so that the right-hand sides of equations (2.9) - (2.10) are continuous at a symmetric corner. In order to obtain accurate solutions for jets having such corners, it is essential that the finite difference scheme properly portray this behavior of the differential equations.

Consider, for example, the term $\frac{\partial R}{\partial\theta}\frac{\partial\psi}{\partial\theta}$ which appears in equation (2.9). Assume that the grid is as shown in Figure 2a, with the corner grid point having index i. The discontinuous change in sign of $\partial R/\partial\theta$ at the corner is reflected in the change of sign between D_+R_i and D_-R_i. Similarly, $D_+\psi_i$ and $D_-\psi_i$ are of opposite sign. Thus,

$$\frac{\partial R}{\partial\theta}\frac{\partial\psi}{\partial\theta} \simeq \tfrac{1}{2}(D_+R_i\, D_+\psi_i + D_-R_i\, D_-\psi_i) , \qquad (5.1)$$

which is an accurate approximation to the continuous function $\frac{\partial R}{\partial \theta}\frac{\partial \psi}{\partial \theta}$ on the boundary. Similarly, the squares of β and $\partial\psi/\partial\theta$ are approximated well by the average of the squares of the one-sided differences. In fact, if R and ψ each have one-sided second derivatives at the corner which are continuous and one-sided third derivatives (which may be discontinuous but bounded), then the above approximations are formally second-order accurate. We note, however, that the central difference approximations to $\frac{\partial R}{\partial \theta}$ and $\frac{\partial \psi}{\partial \theta}$ about the corner point vanish and thus give inaccurate approximations. Also, if the grid points are placed symmetrically about the corner without having a grid point at the corner, as in Figure 2b, then for those grid points nearest the corner the approximation (5.1) will not be accurate. Central differences will not be accurate in this case either.

Consider now the treatment of these terms in the MacCormack scheme (3.4) - (3.5) when the grid is as in Figure 2a. As noted above the approximations such as (5.1) are formally second-order accurate at such corners if R and ψ satisfy appropriate conditions on their one-sided higher derivatives. This implies that equations (3.10) and (3.11) are valid and, hence, that the MacCormack scheme is formally second-order accurate even at such corners (see also section 7).

Laplace's equation in the form of equation (2.11) also contains the terms β^2 and $\frac{\partial}{\partial \rho}(\beta\frac{\partial \psi}{\partial \theta})$. The particular form of differencing for these terms in the difference approximation (3.6)-(3.7) was chosen in light of the above considerations. Therefore, one would expect that the approximation (3.6)-(3.7) is more accurate than if centered differences were used for the derivatives with respect to θ.

6. Examples

Several examples of thin streams falling vertically through an orifice of a specified shape were calculated using the scheme outlined in the previous sections. We present here three of these examples. These and other examples are discussed in more detail elsewhere (see Geer and Strikwerda (1980)). For each example the initial conditions were $\psi \equiv 0$ and $R(\theta,z)$, i.e. $S(\theta,z)$, specified at $z = 0$. Note that the condition $\psi = 0$ at $z = 0$ corresponds to a jet that is emanating with a uniform velocity profile. Thus, in the notation of section 3, we set $z = 0$, $\psi^0_{i,j} = 0$, and $R^0_i = R^0(\theta_i)$, where $R^0(\theta)$ was specified by one of the following:

1. An ellipse, $R^0 = \frac{1}{2}(.25\cos^2\theta + \sin^2\theta)^{-1}$, where the semi-axes of the ellipse are 2 and 1 (Figure 3).

2. An equilateral triangle, $R^0 = \frac{1}{2}\min_{\ell=0,1,2} \sec^2(\theta - 2\pi\ell/3)$ where the length of the side of the triangle is $2\sqrt{3}$. (Figure 4)

3. A rectangle, $R^0 = \frac{1}{2}\min(\sec^2\theta, 4\csc^2\theta)$, where 2 and 4 are the lengths of the sides of the rectangle (Figure 5).

For each example the origin was located at the center of mass of the shape as required in the derivation of the basic equation (2.3) - (2.4) (see Geer (1977a)). The corresponding figures show cross-sections of the jet as several values of z.

The primary purpose of the first example, the ellipse, was to check the accuracy of the numerical scheme. The numerical solution was compared with the analytic solution presented by Geer (1977a). The calculation of this analytic solution involved only the straightforward numerical integration of nonlinear ordinary differential equations, and consequently we assumed that this solution is known exactly.

Figure 3 shows the cross-sectional shape of the jet at various values of z. At $z = 0$, the ellipse had an aspect ratio of 2. As z increased, the shape of the jet became less eccentric, was nearly circular at about $z = 4.9$, and then assumed an elliptical shape with the direction of the major and minor axes exactly interchanged with those of the original axes. The cross-sectional shape became more and more elongated as z increased. At $z = 14.0$, the numerical solution with $N = 101$, $M = 31$, and $\Delta z = .1$ agreed with the analytic solution to within 1% relative error in the ℓ^2- and ℓ^1- norms, and to within 2% relative error in the maximum norm.

In all of our examples the computations terminated when the outward moving portions became sufficiently elongated so that they could no longer be resolved adequately by the uniform grid used for the angular coordinate. The numerical break-up of the solution occurred soon after the last cross-section shown in each case. The conservation law (2.12) was satisfied to within .5% relative error in all the cases shown here.

The other examples had for initial shapes an equilateral triangle (Figure 4) and a rectangle (Figure 5). The initial length of a side of the triangle was $2\sqrt{3}$ units, while the sides of the rectangle were 4 units and 2 units. In these examples, for small values of z the cross-sections decreased in area, but maintained essentially the same shape. In particular the discontinuities in the slopes at the corners were propagated for some distance in z. For larger values of z the shape became non-convex as those portions of the surface that had been corners "buckled-in". Those portions of the surface that had originally been the sides formed the new extremities of the cross-sectional shape. For the case of the equilateral triangle the extremities all extended outward

as z increased. For the case of the rectangle the major extremities extended outward and the minor extremities moved slowly inward. The numerical break-up of these cases occurred along these outward moving extremities as noted above.

We point out that the results for the equilateral triangle are consistent with those of Bidone discussed by Rayleigh (1879), i.e."...a vein issuing from an orifice in the form of a regular polygon, of any number of sides, resolved itself into an equal number of thin sheets, whose planes are perpendicular to the sides of the polygon." (See also Rayleigh (1945).)

However, Rayleigh (1879) implies by the sketch of the cross-sections of the equilateral triangle that the triangle assumed a hexagonal cross-section. Our calculations did not produce such a shape and we presume that this discrepancy is due to mistaken observations near the point where the cross-section was circular.

The example with the rectangular initial shapewas run with $N = 81$, $M = 31$, and $\Delta z = 0.1$. The triangular shape was run with $N = 61$, $M = 31$, and $\Delta z = 0.1$. In these examples, the value of N was chosen so that a grid point would be at or very near the corner of the original shape.

7. Numerical Accuracy

As shown in sections 3 and 5, the finite difference formulas used to approximate the system of equations (2.9) - (2.11) are all formally second-order accurate. Moreover, in the numerical calculations, the parameter Δz and the convergence criteria for the SOR iterations were all chosen with the purpose of maintaining the second-order accuracy. Nonetheless, it must be demonstrated that the overall scheme is in fact second-order accurate.

A series of computations was made to determine the accuracy of the scheme. As noted in section 6, an alternative procedure can be employed to determine the shape of the jet when the jet emanates from an elliptical orifice. This alternative procedure requires solving a nonlinear ordinary differential equation of second order for the aspect ratio. This equation was integrated using a fourth order Runge-Kutta method with a small step size. Because of the high accuracy employed, the numerical solution of this equation was assumed to be exact for the purposes of this comparison.

The difference scheme given by equations (3.1) - (3.8) was used to compute the shape of the elliptical jet (with the initial data given in example 1 of section 6) up to $z = 10.0$ for various values of N and M. The z-step, Δz, was chosen as $10/(N-1)$ so that integrating the finite difference scheme to $z = 10$ required $N-1$ complete steps. The SOR convergence parameter ϵ was 10^{-5}, while the values of N were 21, 41, 61, 81, and 101 and the values of M were $.3(N-1) + 1$.

The results are displayed in Table II for the errors measured in the ℓ^2- and maximum norms. The last two columns give the change in the logarithm of the error divided by the change in the logarithm of $(N-1)$ for successive values of N, i.e.

$$\frac{\log (.0116) - \log (.0536)}{\log 40 - \log 20} = -2.21 \quad , \text{etc.}$$

The closeness of these entries to -2 indicates that the overall method is second-order accurate. The ℓ^2-norm errors listed are relative errors, i.e. the ℓ^2-norm error divided by the ℓ^2-norm of the solution.

Comparisons were also made to study the effect of the placement of grid points on the computation of jets with corners. As discussed in

section 5, the placement of grid points, as shown in Figure 2a should be more accurate than that shown in Figure 2b. In those cases without a grid point at the vertex (Figure 2b) the discontinuities in the tangents were smeared out almost immediately; otherwise, the solutions are similar to those seen in Figures 4 and 5. We emphasize that for such shapes we have no means of ascertaining which solution is more accurate. However, in view of the analysis given in section 5, it would appear that the results are most accurate when a grid point is at or very close to the vertex of the corner.

We note also that the symmetry of the results shown in Figures 3 - 5 is not imposed on the computations but results only from the initial symmetry at $z = 0$. By alternating the forward-backward MacCormack scheme with the backward-forward scheme, asymmetric discretization errors are presumably minimized. However, in runs with the elliptical jet using only the forward-backward scheme, the accuracy and symmetry were not severely affected.

8. Well-posedness of the Problem

We will now discuss the well-posedness of the system of equations (2.9) - (2.11). In particular, we shall derive a necessary condition to insure the growth rate of small perturbations to the solution of equations (2.9) - (2.11) is bounded. We will then indicate how, by a similar analysis, we could demonstrate the stability of our numerical scheme.

An analysis of the well-posedness of the system (2.9) - (2.11) is necessary because the original problem, before the perturbation in the slenderness ratio, is an elliptic problem. Solving such a problem by marching in any particular direction is not a well-posed method. It must then be shown that to solve the equations (2.9) - (2.11) by marching in the z-direction is a well-posed problem.

To begin our analysis, let $(\bar{R},\bar{\psi})$ be a smooth solution of the system (2.9) - (2.11) and consider another solution (R,ψ) of this system of the form

$$R = \bar{R} + 2\eta\tilde{R}\tilde{R}$$

and (8.1)

$$\psi = \bar{\psi} + \eta\tilde{\psi} \ .$$

Here η is a perturbation parameter and $(2\eta\tilde{R}\tilde{R},\eta\tilde{\psi})$ represent small perturbations in $\bar{R}$ and $\bar{\psi}$, respectively. Thus, to investigate the well-posedness of the system (2.9) - (2.11), we shall first determine (to first order) the system of equations satisfied by $(\tilde{R},\tilde{\psi})$. We shall then show that this linear system is well-posed if a certain scalar quantity $\alpha = \alpha(\theta,z)$ is non-positive.

In order to determine the equations satisfied by $(\tilde{R},\tilde{\psi})$, we substitute (8.1) into (2.9) - (2.11), expand the resulting expressions in a Taylor series about $\eta = 0$, and then set the coefficient of η in each equation equal to zero. In this way we obtain the following system of equations.

$$2\bar{R}\frac{\partial\tilde{R}}{\partial z} = (1+\bar{\beta}^2)\frac{\partial\tilde{\psi}}{\partial\rho} - \bar{\beta}\frac{\partial\tilde{\psi}}{\partial\theta} + (2\bar{\beta}\frac{\partial\bar{\psi}}{\partial\rho} - \frac{\partial\bar{\psi}}{\partial\theta})\frac{\partial\tilde{R}}{\partial\theta}$$
$$-2\frac{\partial\bar{R}}{\partial z}\tilde{R} \ , \tag{8.2}$$

$$2\bar{R}\frac{\partial\tilde{\psi}}{\partial z} = (1+\bar{\beta}^2)\frac{\partial\bar{\psi}}{\partial\rho}\frac{\partial\tilde{\psi}}{\partial\rho} - \frac{\partial\bar{\psi}}{\partial\theta}\frac{\partial\tilde{\psi}}{\partial\theta} + \bar{\beta}(\frac{\partial\bar{\psi}}{\partial\rho})^2\frac{\partial\tilde{R}}{\partial\theta}$$
$$-(4\bar{R}\frac{\partial\bar{\psi}}{\partial z} + \frac{3}{2}\frac{\bar{R}^2}{(1+z)^2})\tilde{R} \ , \tag{8.3}$$

$$(1+\bar{\beta}^2)\,\frac{1}{\rho}\,\frac{\partial}{\partial\rho}\,(\rho\frac{\partial\tilde{\psi}}{\partial\rho}) - \frac{\partial\bar{\beta}}{\partial\theta}\,\frac{1}{\rho}\,\frac{\partial\tilde{\psi}}{\partial\rho} + \frac{1}{\rho^2}\,\frac{\partial^2\tilde{\psi}}{\partial\theta^2} - 2\bar{\beta}\,\frac{1}{\rho}\,\frac{\partial^2\tilde{\psi}}{\partial\rho\partial\theta} =$$

$$-2(\bar{\beta}\,\frac{1}{\rho}\,\frac{\partial}{\partial\rho}\,(\rho\frac{\partial\bar{\psi}}{\partial\rho}) - \frac{1}{\rho}\,\frac{\partial^2\bar{\psi}}{\partial\rho\partial\theta})\,\frac{\partial\tilde{R}}{\partial\theta} + \frac{1}{\rho}\,\frac{\partial\bar{\psi}}{\partial\rho}\,\frac{\partial^2\tilde{R}}{\partial\theta^2} \tag{8.4}$$

where $\bar{\beta} = \frac{1}{2\bar{R}}\,\frac{\partial\bar{R}}{\partial\theta}$. Here equations (8.2) - (8.3) hold on $\rho = 1$, while equation (8.4) holds for $0 \le \rho < 1$ and $0 \le \theta \le 2\pi$.

We now wish to examine the behavior of $(\tilde{R},\tilde{\psi})$ in the neighborhood of a point (θ_0,z_0) on the boundary $\rho = 1$. We are particularly interested in the behavior as a function of z of solutions $(\tilde{R},\tilde{\psi})$ which have high frequency components in the angular variable θ. Thus, we shall consider solutions whose initial values at $z = z_0$ are of the form

$$\tilde{R}(\theta,z_0) = e^{i\omega\ell_1(\theta)}R_0(\theta)$$

are similarly for $\tilde{\psi}$, where ω is a positive parameter and ℓ_1 is a function of θ. We will then construct a formal asymptotic series for $(\tilde{R},\tilde{\psi})$ in positive powers of $1/\omega$. This approach is similar to that of Lax (1957).

It is a result of the analysis that powers of ω to half-integer powers enter the expansion in a natural way. Thus, we look for solutions to (8.2) - (8.4) of the form

$$\tilde{R} = e^{i(\omega\ell_1+\omega^{1/2}\ell_{1/2})}\sum_{j=0}^{\infty} R_{j/2}(\theta,z)\omega^{-j/2} \tag{8.5}$$

$$\tilde{\psi} = e^{i(\omega\ell_1+\omega^{1/2}\ell_{1/2})}\sum_{j=0}^{\infty} \{\rho^{\omega k_1+\omega^{1/2}k_{1/2}}\,\psi_{j/2}(\theta,z,\rho) + \hat{\psi}_{j/2}(\theta,z,\rho)\}\omega^{-j/2}\ , \tag{8.6}$$

where $\omega >> 1$ and $\ell_1(\theta,z)$, $\ell_{1/2}(\theta,z)$, $k_1(\theta,z)$, $k_{1/2}(\theta,z)$, $R_{j/2}$, $\psi_{j/2}$, and $\hat{\psi}_{j/2}$ are all functions to be determined. The first term in the brackets in the expansion (8.6) represents a solution to the homogeneous version of equation (8.4) (i.e. equation (8.4) with $\tilde{R} \equiv 0$), while the second term represents a particular solution of this equation corresponding to $\tilde{R}$ given by equation (8.5).

Substituting the expansions (8.5) and (8.6) into equation (8.4) and equating coefficients of like powers of ω results in the relations

$$\hat{\psi}_0 = \rho \frac{\partial \bar{\psi}}{\partial \rho} R_0, \quad \hat{\psi}_{1/2} = \rho \frac{\partial \bar{\psi}}{\partial \rho} R_{1/2}, \tag{8.7}$$

and

$$k_1 = \frac{1}{1 - i\bar{\beta}} \frac{\partial \ell_1}{\partial \theta}, \quad k_{1/2} = \frac{1}{1 - i\bar{\beta}} \frac{\partial \ell_{1/2}}{\partial \theta}, \tag{8.8}$$

$$\text{if} \quad \frac{\partial \ell_1}{\partial \theta} \geq 0, \quad \text{and}$$

$$k_1 = -\frac{1}{1 + i\bar{\beta}} \frac{\partial \ell_1}{\partial \theta}, \quad k_{1/2} = -\frac{1}{1 + i\bar{\beta}} \frac{\partial \ell_{1/2}}{\partial \theta} \tag{8.9}$$

$$\text{if} \quad \frac{\partial \ell_1}{\partial \theta} < 0 .$$

In the following we will assume, without loss of generality, that $\partial \ell_1 / \partial \theta$ is non-negative since by taking the complex conjugate of (8.5) and (8.6) we obtain a solution of similar form with $\partial \ell_1 / \partial \theta$ of opposite sign.

We now substitute the expansions (8.5) and (8.6) into equations (8.2) and (8.3) and equate like powers of ω, using the relations (8.7) and (8.8). The terms containing first powers of ω give the equations

$$2\bar{R} R_0 \left(\frac{\partial \ell_1}{\partial z} - \lambda \frac{\partial \ell_1}{\partial \theta}\right) = \psi_0 \frac{\partial \ell_1}{\partial \theta}$$

$$2\bar{R} \psi_0 \left(\frac{\partial \ell_1}{\partial z} - \lambda \frac{\partial \ell_1}{\partial \theta}\right) = 0$$

where $\lambda = (\bar{\beta}\,\frac{\partial\bar{\psi}}{\partial\rho} - \frac{\partial\bar{\psi}}{\partial\theta})/2\bar{R}$.

From this we conclude that $\psi_0 \equiv 0$ and

$$\frac{\partial \ell_1}{\partial z} - \lambda\,\frac{\partial \ell_1}{\partial \theta} = 0 \ . \tag{8.10}$$

The terms with $\omega^{1/2}$ give the equation

$$\frac{\partial \ell_{1/2}}{\partial z} - \lambda\,\frac{\partial \ell_{1/2}}{\partial \theta} = -\frac{i}{2\bar{R}}\,\frac{\partial \ell_1}{\partial \theta}\,\frac{\psi_{1/2}}{R_0} \ . \tag{8.11}$$

Equation (8.10) is similar to the eikonal equation of geometrical optics, and in particular it shows that ℓ_1 which is initially real will remain so, being constant along the characteristics given by

$$\frac{d\theta}{dz} + \lambda(\theta,z) = 0.$$

Thus this system has real characteristics as do hyperbolic systems. From equation (8.11) we see that $\ell_{1/2}$ will not be real unless $\psi_{1/2}\,R_0$ is purely imaginary. If

$$\text{Im}\ \ell_{1/2}(z,\theta) < 0$$

then from equation (8.5) we see that the amplitude of the solution will grow as

$$e^{-\omega^{1/2}\ \text{Im}\ \ell_{1/2}}$$

and, thus, the initial value problem for equations (8.2) and (8.3) will be ill-posed in the sense of Hadamard (see Kreiss (1963)).

From the zero-th order terms in ω we obtain the relation

$$\frac{\partial \ell_1}{\partial \theta}\left(\frac{\psi_{1/2}}{R_0}\right)^2 = 2\bar{R}\alpha \tag{8.12}$$

where

$$\alpha = \lambda \frac{\partial^2 \bar{\psi}}{\partial \rho \partial \theta} - 2\frac{\partial \bar{\psi}}{\partial z} - \frac{3}{4} \frac{\bar{R}}{(1+z)^2} - \frac{\partial^2 \bar{\psi}}{\partial \rho \partial z} + \frac{1}{R} \frac{\partial \bar{R}}{\partial z} \frac{\partial \bar{\psi}}{\partial \rho} .$$

Thus, we see that if α is non-positive then $\psi_{1/2}/R_0$ will be purely imaginary and the amplitude of the solution will not grow with ω, while if α is positive then the high frequency perturbations will grow exponentially as $e^{\omega^{1/2}|\text{Im } \ell_{1/2}|}$. Thus, it is a necessary condition for well-posedness that α be non-positive.

In the numerical experiments the quantity α was approximated using (formally) first-order accurate one-sided differences. It was found that this approximation to α was negative throughout most of the computation. At those values of z for which the thin sheets were not being adequately resolved, α became positive. However, the solution was not smooth so that the computation of α may have been so inaccurate as to be meaningless.

It appears then that the system of equations (2.9-2.11) is well-posed for each of the examples considered here, at least for those values of z for which the solution has been computed. We conjecture that is is well-posed for all values of z. We believe that the break-up of the numerical solution is purely a numerical phenomena, caused by inadequate resolution, and not caused by a loss of well-posedness of the differential equations.

As a demonstration of the similarity of our system to hyperbolic systems, we numerically integrated the system with the initial data of example 2 from $z = 0$ to $z = 2$ and then integrated back to $z = 0$. The initial conditions were recovered to within the numerical accuracy of the method. Thus this system is reversible as are hyperbolic systems.

Finally, we offer the following comments on the stability of the difference scheme which is described in section 3. As in the above discussion of the well-posedness of the differential equations, all that

can be done is to analyze the stability of the linearized problem. The analysis of the stability of the linearized system mimics the above analysis of the well-posedness although it involves more complicated algebraic expressions. The amplification factor of the von Neumann analysis corresponds to the factor $e^{i(\omega \ell_1 + \omega^{1/2} \ell_{1/2})}$. The actual details of the derivation are omitted in the interests of brevity.

References

Garabedian, P. 1956 "Estimation of the Relaxation Factor for Small Mesh Sizes," Math Tables and other Aids to Comp. 10, 183-185.

Geer, J. F. 1977a "Slender streams with gravity: Outer asymptotic expansions I," *Phys. Fluids*, 20, 1613-1621.

Geer, J. F. 1977b "Slender streams with gravity: Outer asymptotic expansions II," *Phys. Fluids*, 20, 1622-1630.

Geer, J. F. and Strikwerda, J. C. "Vertical slender jets" *J. Fluid Mech.* (to appear).

Green, A. E. 1977 "On the steady motion of jets with elliptical sections," *Acta Mech.*, 26, 171-177.

Kreiss, H. O. 1963 "Über Sachgemässe Cauchyprobleme," *Math. Scand.* 13, 109-123.

Lax, P. D. 1957 "Asymptotic solutions of oscillatory initial value problems," *Duke Math. J.*, 24, 627-646.

MacCormack, R. W. 1969 "The effect of viscosity in hypervelocity impact cratering," AIAA Hypervelocity Impact Conference, April 1969, AIAA Paper No. 69-354.

Rayleigh, Lord 1879 "On the capillary phenomena of jets," Proc. Roy. Soc., 29, 71-97.

Rayleigh, Lord 1945 The Theory of Sound, 2nd. edition, Dover.

Tuck, E. O. 1976, "The shape of free jets of water under gravity," *J. Fluid Mech.*, 76, 625.

Wilson, D. G., Solomon, A. D., and Boggs, P. T. 1978 Moving Boundary Problems, Academic Press (New York).

Table I

SOR iterations for several values of z for a rectangle 81×31, $\Delta z = .1$

z	a. Linear extrapolation Eq. (4.8) Iterations Predictor/Corrector		b. Previous value Eq. (4.11) Iterations Predictor/Corrector	
1.0	75	75	>250	48
2.0	22	23	>250	26
3.0	13	13	>250	16
4.0	12	11	247	12
5.0	14	12	217	15
6.0	14	13	181	15
7.0	14	13	147	17

Table II

Analysis of the error and accuracy of the method for elliptical jets.

N-1	ℓ^2 error	max error	ℓ^2 order	ℓ_∞ order
20	5.36×10^{-2}	2.00×10^{-1}	-	-
40	1.16×10^{-2}	2.93×10^{-2}	-2.21	-2.77
60	5.15×10^{-3}	1.12×10^{-2}	-2.00	-2.37
80	2.89×10^{-3}	5.93×10^{-3}	-2.01	-2.21
100	1.85×10^{-3}	3.74×10^{-3}	-2.00	-2.07

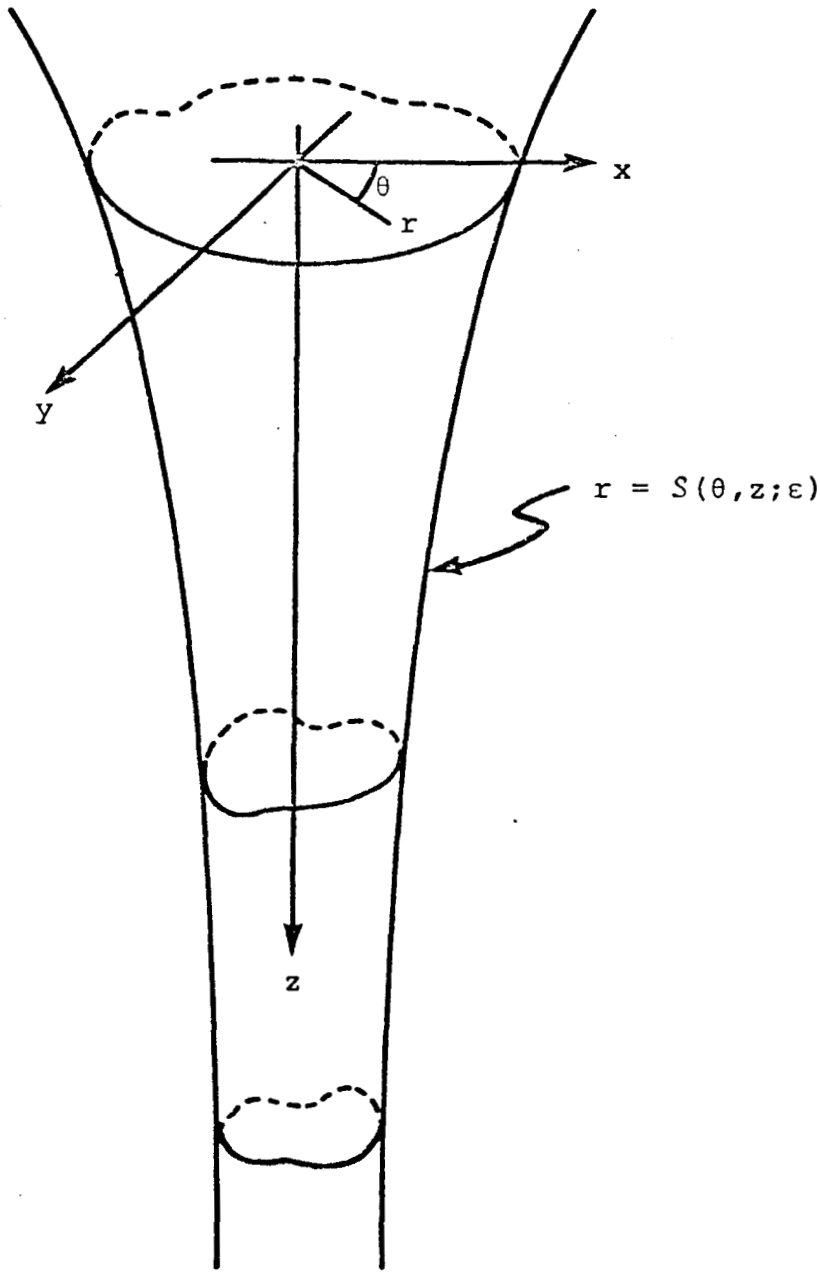

Figure 1. Sketch of a vertical slender jet, with an indication of the coordinate system. The locus of centroids of the cross-sections of the jet form a straight line (in the direction of gravity), which we choose to be the z-axis. Then r, θ, and z form the usual cylindrical coordinate system, where θ is measured from any convenient plane through the z-axis. The free surface of the jet is denoted by $r = S(\theta,z;\varepsilon)$.

Figure 2. Examples of the placement of gridpoints near a corner.

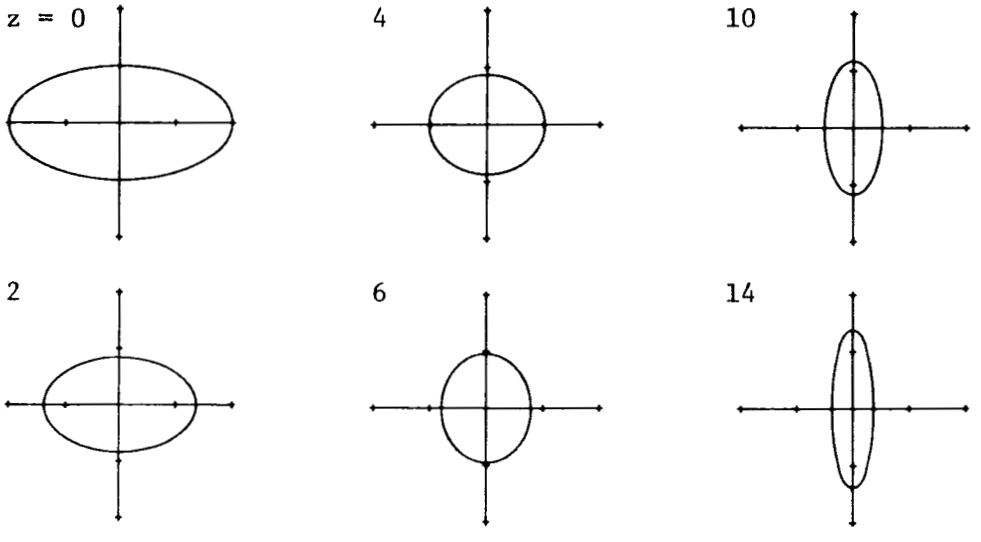

Figure 3. Cross-sectional shapes at several values of z for a jet with an initial shape of an ellipse.

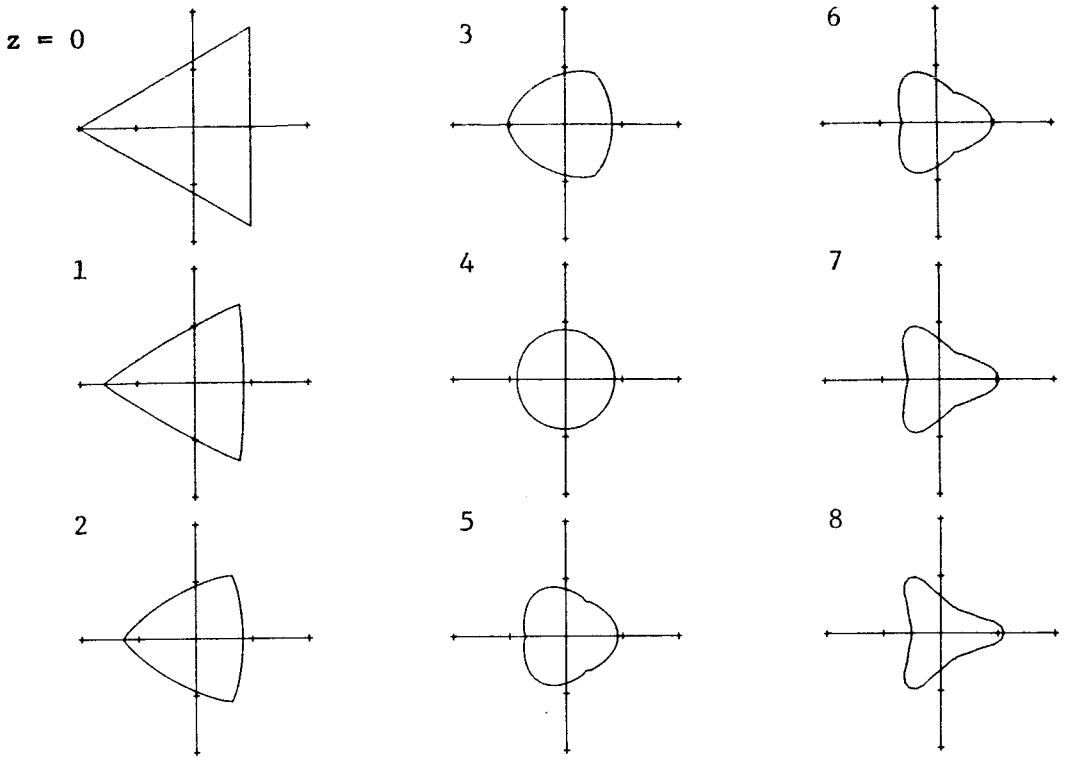

Figure 4. Cross-sectional shapes at several values of z for a jet with the initial shape of an equilateral triangle, with side of length $\sqrt{3}$.

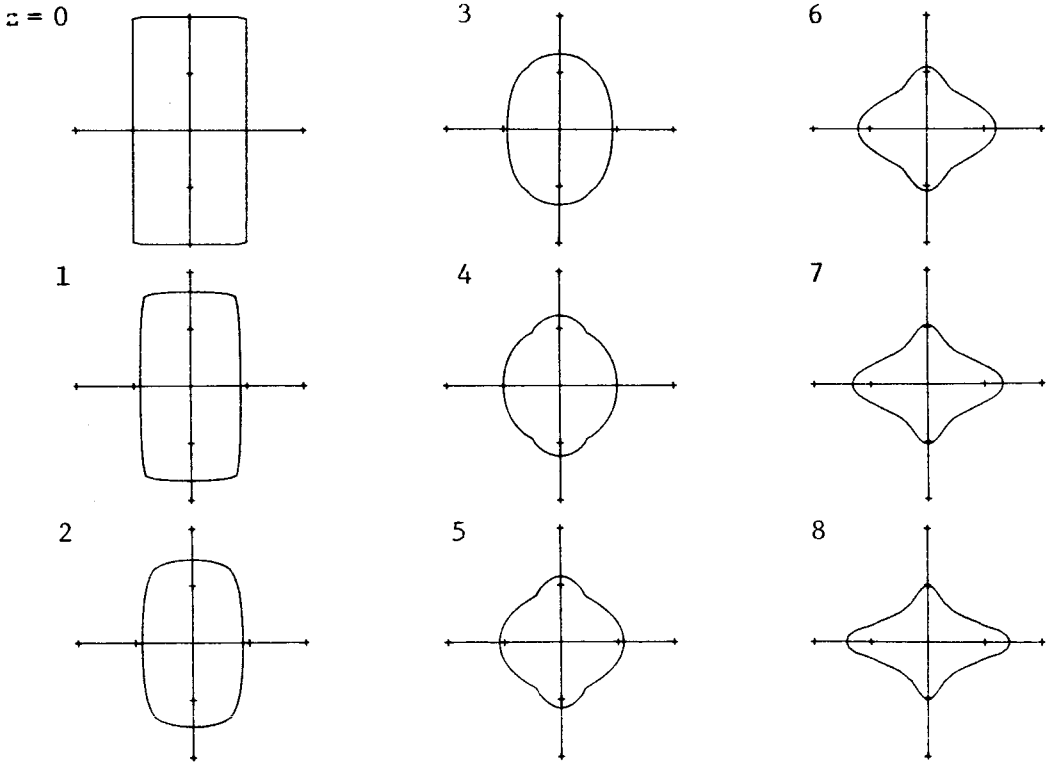

Figure 5. Cross-sectional shapes for a jet with the initial shape of a rectangle with sides of length 2 and 4.

Figure Captions

1. Sketch of a vertical slender jet, with an indication of the coordinate system. The locus of centroids of the cross-sections of the jet form a straight line (in the direction of gravity), which we choose to be the z-axis. Then r, θ, and z form the usual cylindrical coordinate system, where θ is measured from any convenient plane through the z-axis. The free surface of the jet is denoted by $r = S(\theta,z,\varepsilon)$.

2. Examples of the symmetric placement of grid points near a corner. In example (a) a grid point is placed at the vertex, while in example (b) the corner lies between two grid points.

3. Cross-sectional shapes at several values of z for a jet with an initial shape of an ellipse.

4. Cross-sectional shapes at several values of z for a jet with the initial shape of an equilateral triangle, with side of length $2\sqrt{3}$.

5. Cross-sectional shapes for a jet with the initial shape of a rectangle with sides of length 2 and 4.